Chelated Nitrogen-Sulphur Codoped TiO_2: Synthesis, Characterization, Mechanistic and UV/visible Photocatalytic Studies

Hayat Khan[*1,2], Imran Khan Swati[2], Mohammad Younas[2], Asmat Ullah[2]

Supplementary Information

S.1. Thermal gravimetric analysis (TGA).

Thermal gravimetric analysis were adopted to evaluate the thermal properties of the undoped and NS codoped TiO_2 powders before calcination. Figure S1 shows the TGA/DTGA curves of (a) $T_{control}$ (b) T_{FA} and $(NS)_{0.06}$-T_{FA} (c) T_{AA} (c) and (d) $(NS)_{0.06}$-T_{AA} powders, respectively. In the TGA curves, the mass of the sample (M %) is recorded as a function of heating temperature; in the DTGA curve, the first derivative of TGA curve is ascribed as a function of temperature and its maximum peaks show very accurately the temperature values where any process of partial mass loss has taken place. In TGA curves; a total weight loss of 30.7% ($T_{control}$), 17.5% (T_{FA}, $(NS)_{0.06}$-T_{FA}), 8.3% (T_{AA}) and 17.5% ($(NS)_{0.06}$-T_{AA}) was recorded between the temperature span of 25 ^oC to 800 ^oC. This total weight loss occurred at different temperatures during the heating process as depicted in the DTGA curves. In all the powders the peaks below 100 ^oC is attributed to the evaporation of ethanol and chemically adsorbed water molecules from the TiO_2 surface [1] surface. However, the evaporation process occurs earlier in T_{FA} and $(NS)_{0.06}$-T_{FA} (49.4 ^oC), T_{AA} (59.6 ^oC), $(NS)_{0.06}$-T_{AA} (48.7 ^oC) compared to $T_{control}$ (71.2 ^oC) powders due to the chelation of formate and acetate group with titanium precursor. The peak at 373 ^oC in $T_{control}$ powder is attributed to a phase change from amorphous to anatase powder while this transformation temperature is observed in the modified TiO_2 powder at 228.8 ^oC (T_{FA}), 275.1 ^oC ($(NS)_{0.06}$-T_{FA}) and 360.8 ^oC ($(NS)_{0.06}$-T_{AA}) implying that due to carboxylic acid chelation and NS codoping crystalline anatase formation is occurring at lower temperature. This result further indicates the stability of anatase phase which could be converted to rutile at extended temperature compared to $T_{control}$ powder where due to powder amorphous nature anatase is converted to rutile at lower temperature. Moreover, the highest weight loss in the $T_{control}$ powder further clarify the weakened gel structure formation which collapse rapidly on calcination forming rutile at lower temperature. The peaks appear at 181.4 ^oC (T_{FA}), 189.1 ^oC (T_{AA}), 171.2 and 253.1 ^oC ($(NS)_{0.06}$-T_{AA}) may represent the removal of carboxylic acid or ascribed to the thermal decomposition of residual organic groups or to the dehydroxylation. Furthermore, in the TGA curves, after 500 ^oC weight loss started to remain constant, which illustrate that 500 ^oC is an appropriate and ideal calcination temperature for synthesizing crystalline TiO_2.

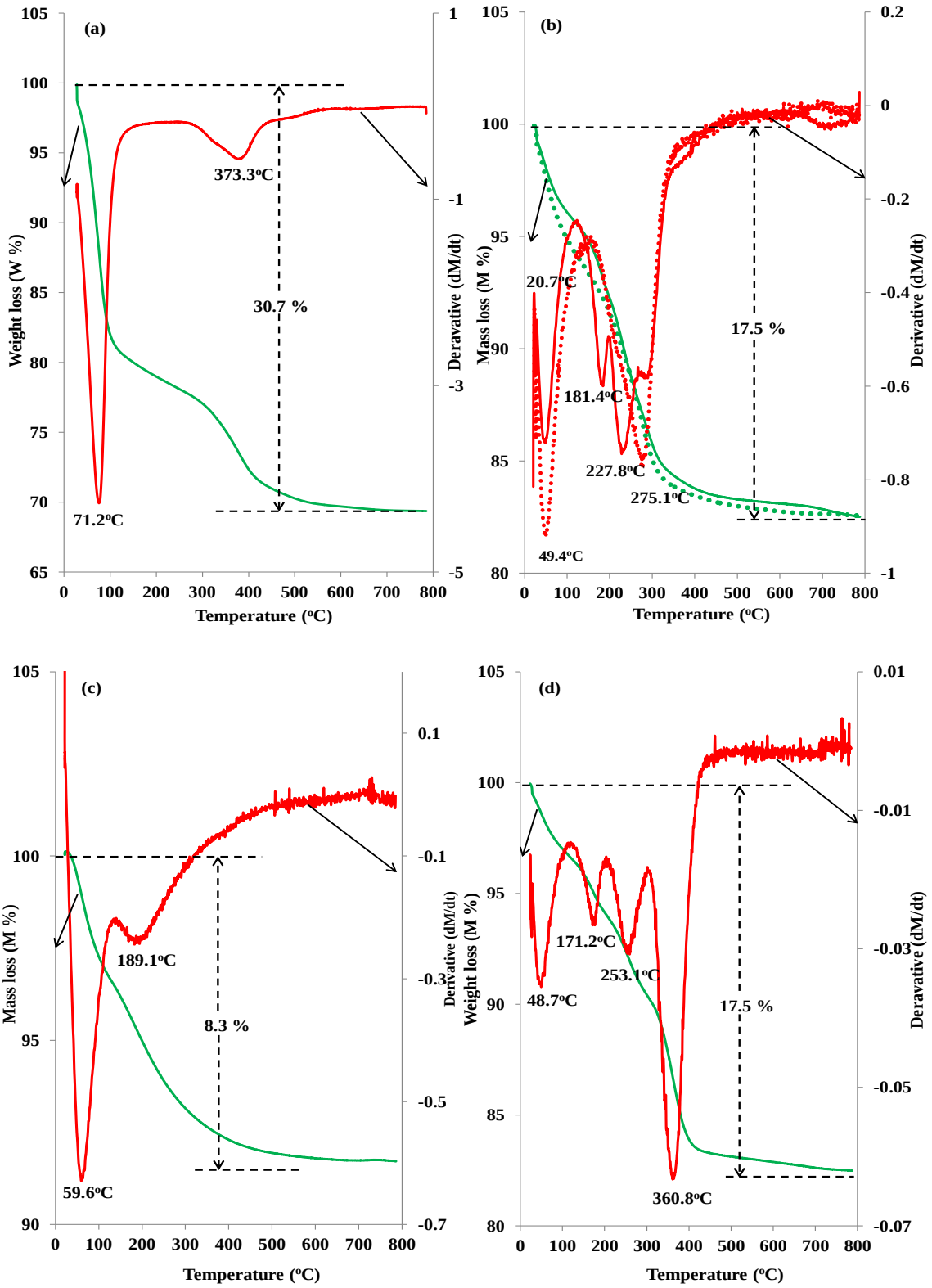

Figure S1: TGA/DTGA curves of (a) $T_{control}$ (b), T_{FA} and $N_{0.06}$-T_{FA} (c), T_{AA} and (d) $N_{0.06}$-T_{AA} powders, respectively.

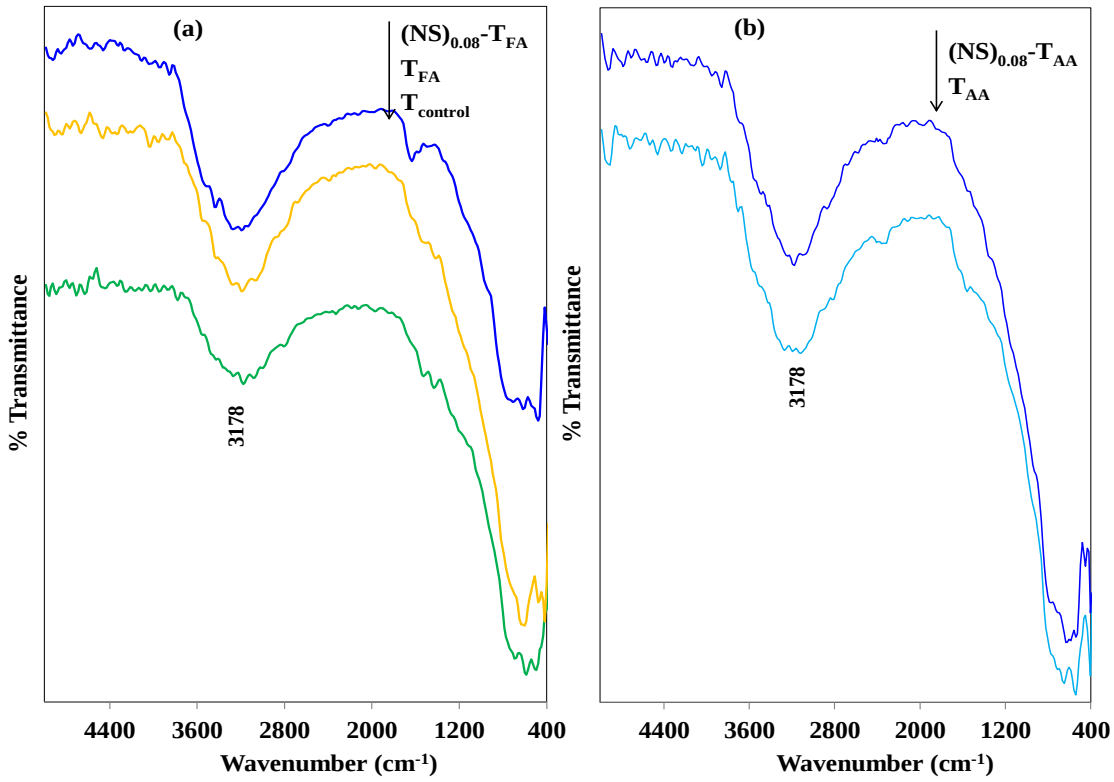

Figure S2: FTIR spectra of calcined powders at 700 ^{o}C (a) $T_{control}$, T_{FA} and $(NS)_{0.08}$-T_{FA}, (b) T_{AA} and $(NS)_{0.08}$-T_{AA}.

S.2. Photoluminescence (PL) Spectroscopy.

PL analysis has given a great deal of attention in the field of photocatalysis, because PL emission spectra not only help to understand the fate of photogenerated electron hole pairs (charge carrier trapping and recombination), but, also give information regarding lattice defects (self-trapped excitons, oxygen vacancies (OV_s) and surface states. PL emission mainly results from the radiative recombination of electrons and holes either directly via band-band or indirectly via band gap states [2]. Higher PL intensity indicates an increased recombination rate of electrons and holes, implying lower separation efficiency and decreased photocatalytic activity [3-5]. Figure S3 shows the room temperature PL spectra of the powders (T_{FA}, $(NS)_{0.06}$-$T_{FA,}$ $(NS)_{0.08}$-$T_{FA,}$ $(NS)_{0.1}$-T_{FA}) excited with two different wavelengths 310 and 410 nm, respectively. The emission spectra of the powders excited at 310 nm consist of a UV shoulder at 396 nm, four violet emission peaks at 412, 418, 437 and 449 nm, six blue emission peaks at 456, 461, 466, 471, 479 and 490 nm and one green emission peak at 559 nm, while the emission spectra obtained at excitation wavelength of 410 nm shows peaks at 542 nm (green emission peak), 610 nm (orange emission peak) and 663 nm (red emission peak), respectively. Table S1 illustrates the explanation of these peaks;

Table S1 Observed peaks explanation for PL spectra of T_{FA} and $(NS)_x$-T_{FA}.

Peak	Assignment
396	attributed to the phonon assisted indirect transmission from the center of Brillouin zone to the edge (Γ_3 to X_{1b}) [6].
412	assigned to free excitons [7].
418	ascribed to the phonon assisted indirect transition, but from the edge to the center of the Brillouin zone (X_{1a} to Γ_{1b}) [6].
437	attributed to self-trapped excitons localized on TiO_6 octahedra [8, 9].
450	excitons transition from isolated N 2p level to the conduction band of TiO_2 [10].
456	related to surface states or oxygen related defect states [11].
460	oxygen vacancy with one trapped electrons (F^+ color center) [12].
466	oxygen vacancy with two trapped electrons (F color centre) [13].
471	ascribed to band edge emission or related to crystal defects such as oxygen vacancies or interstitial sites in TiO_2 and or the free $O^{2-} \rightarrow Ti^{4+}$ charge transfer transition.
479	attributed to charge transfer transition from Ti^{+3} to oxygen anion in a TiO_6^{8-} complex associated with surface oxygen vacancies [14].
490	related to the formation of oxygen defect states (TiO_{2-x}) located near the bottom of the conduction band [12].
560	associated with transitions of electrons from the conduction band edge to deep trap holes owing to oxygen vacancies.
542	appears due to structural defects, which may be attributed to native defects and impurities such as Ti interstitials and oxygen vacancies or from the recombination process of the excited holes and electrons in a self-trapped excited states [13].
610	associated with different types of charged (F, F^+, F^{++}) oxygen vacancies states or may be assigned to the recombination of trapped electrons with valance band holes [15].
663	attributed to deep traps caused by oxygen vacancies or electron trappers with under coordinated $Ti^{4+/3+}$ species [15].

To further understand the PL spectra, the peak at 560 nm vanishes upon switching the excitation wavelength (Figure S3b), which implies that recombination of conduction band electrons with the holes in the deep trap are weakened, because due to low photon energy excitation of electrons to conduction band is minimized. Figure S3c and d shows the intensity ratio of oxygen vacancy for carboxylic acid modified TiO_2 at 460 and 466 nm and oxygen defect states at 490 nm versus dopant concentration, respectively. As observed the intensity of oxygen vacancies (IOV) and oxygen defect states (TiO_{2-x}) are higher in undoped and NS codoped powders employing formic acid compared to acetic acid. This means

that in comparison to acetate $(NS)_x$-TiO_2, the increase formation of oxygen vacancies and defect states in formate $(NS)_x$-TiO_2 result in the transformation of anatase to rutile (Table 1, section 3.1). This result show that due to the presence of oxygen vacancies, space is created within the crystal lattice facilitating the rearrangement of oxide ions with greater ease, which is necessary for the structural changes associated with anatase to rutile transformation [16]. Furthermore, it is also possible that due to the compact structure of the alkoxide precursor (Figure 4b) chemically modified by acetate group compared to the open structure of formate group modified alkoxide precursor (Figure 4a), it may not be easy for the NS dopant atoms to enter into the acetate structure and replaces substitutionaly the oxygen and titanium atoms. As a result, the oxygen vacancy concentration in the samples (T_{AA} and $(NS)_x$-T_{AA}) decreases, which promotes and stabilizes anatase formation towards higher calcination temperature.

The PL intensity of the sample T_{FA} is higher than the NS codoped samples signifying the decrease in the recombination rate upon codoping, because PL spectrum is the outcome of recombination of photogenerated electrons and holes. The effective quenching of the photoluminescence is ascribed to the trapping of photoinduced charge carriers by the dopants ions in addition to oxygen vacancies and surface states ($Ti^{4+/3+}$). The charge carriers on diffusion to the surface generates super oxide anions ($O_2^{-\bullet}$) and hydroxyl radicals ($OH^{\bullet}$) which are necessary for the degradation of aqueous organic compounds. Based on these observations it is expected that due to decrease in PL intensity, NS codoped powders will have enhanced photocatalytic activity than undoped TiO_2 powders.

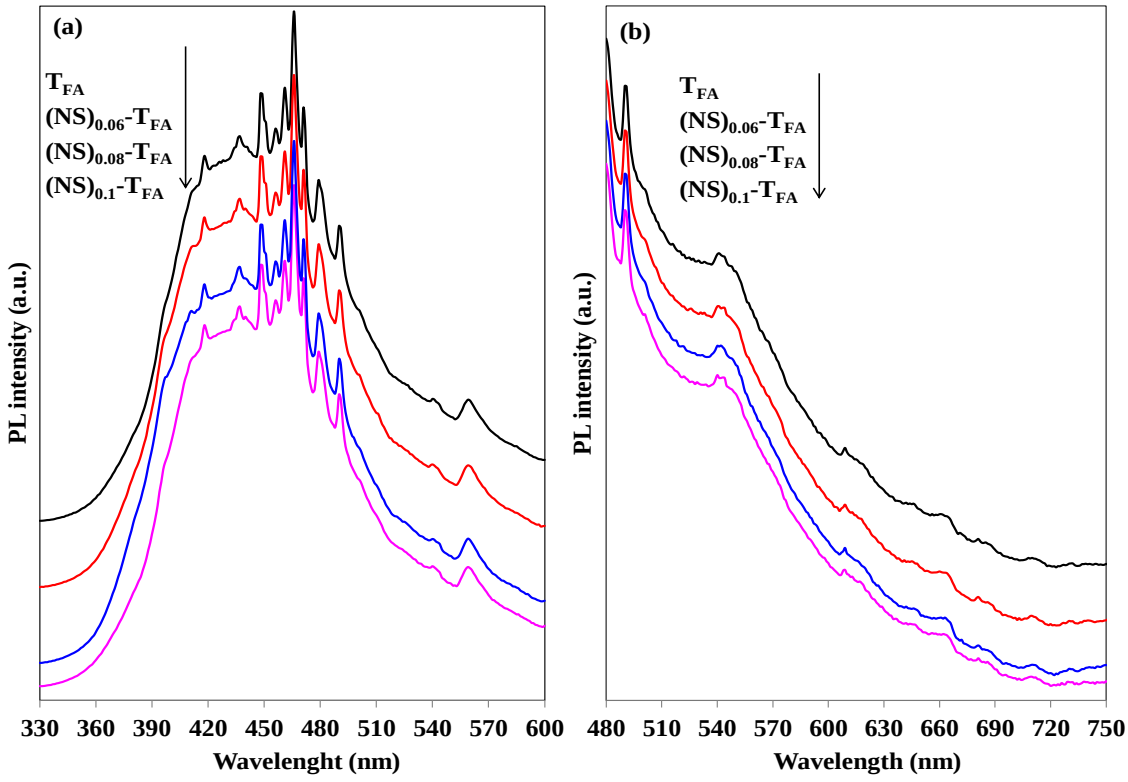

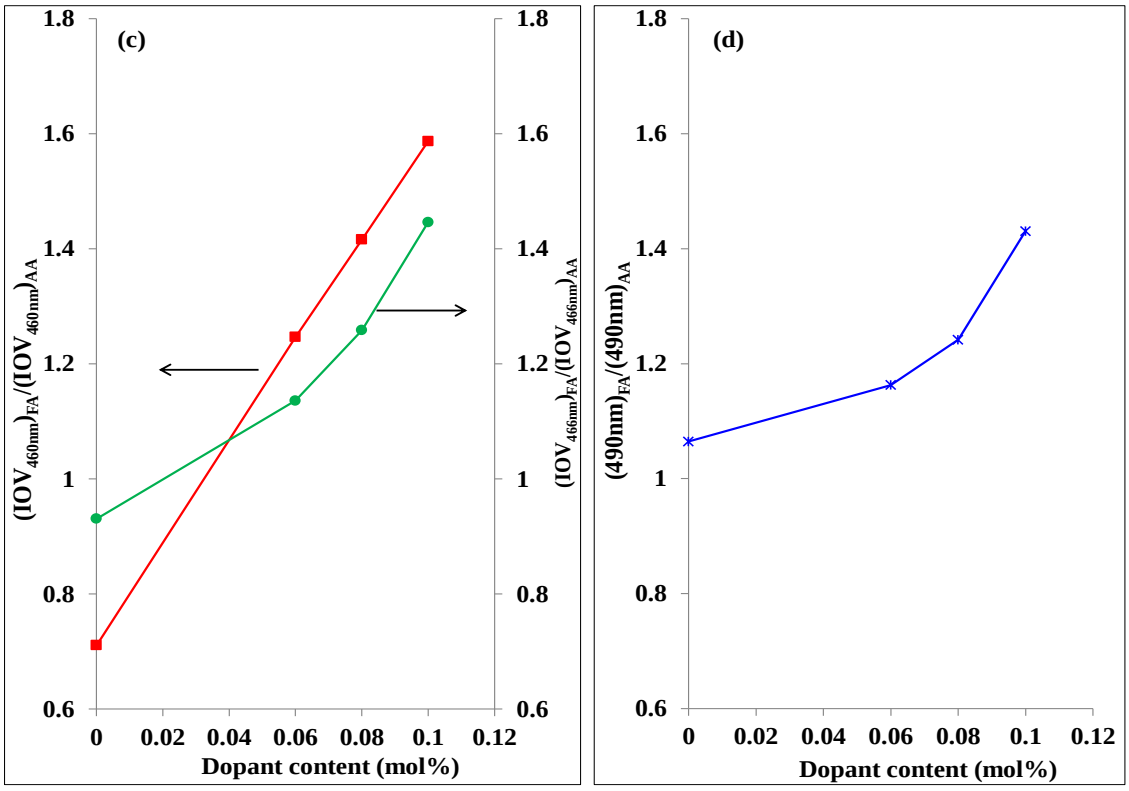

Figure S3: Room temperature PL spectra of T_{FA}, $(NS)_{0.06}$-$T_{FA,}$ $(NS)_{0.08}$-T_{FA} and $(NS)_{0.1}$-T_{FA} powders calcined at 700 ^{o}C and excited at; (a) 310 nm and (b) 410 nm. Intensity ratio of oxygen vacancy in formic acid modified TiO_2 to acetic acid modified TiO_2 versus dopant concentration (c) at 460 (full lines) and 466 nm (dotted lines) and (d) at 490 nm.

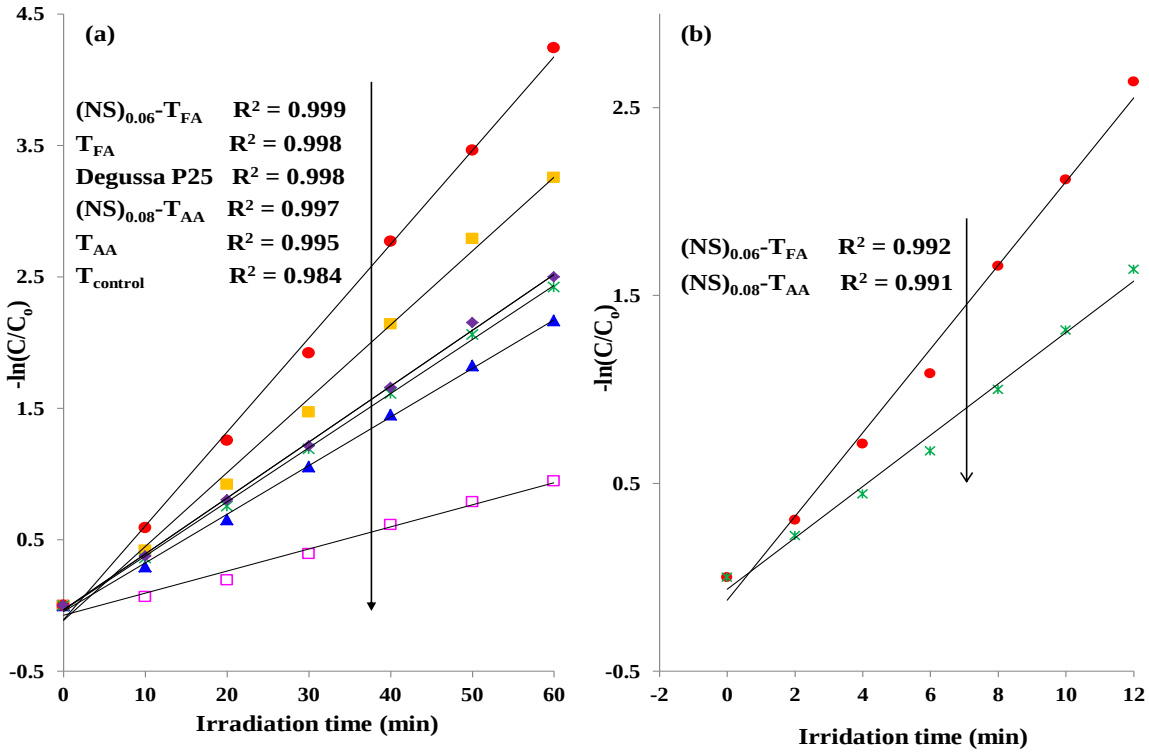

Figure S4: Pseudo first order kinetics of 4-chlorophenol degradation under (a) UV irradiation and (b) visible irradiation for Degussa P25 and the selected photocatalyst powders calcined at 700 ^{o}C.

References

[1] N. Hafizah and I. Sopyan, "Nanosized TiO_2 photocatalyst powder via sol-gel method: effect of hydrolysis degree on powder properties", *International Journal of Photoenergy*, vol. 2009, pp. 1-8, 2009.

[2] F. B. Li, X.Z . Li, C. H. Ao, S. C. Lee and M. F. Hou, "Enhanced photocatalytic degradation of VOCs using Ln^{3+}–TiO_2 catalysts for indoor air purification", *Chemosphere*, vol. 59, no. 12, pp. 787-800, 2005.

[3] Y. F. Li, D. Xu, J. I. Oh, W. Shen, X. Li and Y. Yu, "Mechanistic study of codoped titania with nonmetal and metaliIons: A case of C + Mo codoped TiO_2", *ACS Catalysis*, vol. 2, no. 3, pp. 391-398, 2012.

[4] Y. Cong, J. Zhang, F. Chen and M. Anpo, Synthesis and characterization of nitrogen-doped TiO2 nanophotocatalyst with high visible light activity", T*he Journal of Physical Chemistry C*, vol. 111, no. 19, pp. 6976-6982, 2007.

[5] H. Khan and D. Berk, "Characterization and mechanistic study of Mo^{+6} and V^{+5} codoped TiO_2 as a photocatalyst", *Journal of Photochemistry and Photobiology A: Chemistry*, vol. 294, pp. 96-109, 2014.

[6] N. Serpone, D. Lawless and R. Khairutdinov, "Size effects on the photophysical properties of colloidal anatase TiO_2 particles: size quantization versus direct transitions in this indirect semiconductor? ", *The Journal of Physical Chemistry*, vol. 99, no. 45, pp. 16646-16654, 1995.

[7] Y.X . Zhang, G. H. Li, Y. X. Jin, Y. Zhang, J. Zhang and L. D. Zhang, "Hydrothermal synthesis and photoluminescence of TiO_2 nanowires", *Chemical Physics Letters*, vol. 365, no. 3-4, pp. 300-304, 2002.

[8] J. Xu, S. Shi, L. Li, X. Zhang, Y. Wang, X. Chen, J. Wang, L. Lv, F. Zhang and W. Zhong, Structural, optical, and ferromagnetic properties of Co-doped TiO_2 films annealed in vacuum",, *Journal of Applied Physics*, vol. 107, pp. 053910-05397, 2010.

[9] H. Khan and I. K. Swati, "Fe^{3+}-doped Anatase TiO_2 with d–d transition, oxygen vacancies and Ti^{3+} centers: Synthesis, characterization, UV–vis photocatalytic and mechanistic studies", *Industrial and Engineering Chemistry Research*, vol. 55, no. 23, pp. 6619-6633, 2016.
[10] S. Hu, F. Li and Z. Fan, "A convenient method to prepare Ag deposited N-TiO_2 composite nanoparticles via NH3 plasma treatment", *Bulletin Korean Chemical Society*, vol. 33, no. 7, pp. 2309-1314, 2012.
[11] B. Choudhury and A. Choudhury, "Tailoring luminescence properties of TiO_2 nanoparticles by Mn doping", *Journal of Luminescence*, vol. 136, pp. 339-346, 2013.
[12] H. Khan and D. Berk, "Synthesis, physicochemical properties and visible light photocatalytic studies of molybdenum, iron and vanadium doped titanium dioxide", *Reaction, Kinetics, Mechanisum and Catalysis*, vol. 11, pp. 393-414, 2013.
[13] C. M. Liu, X. T. Zu and W. L. Zhou, "Photoluminescence of nitrogen doped $SrTiO_3$", *Journal of Physics D: Applied Physics*, vol. 40, no. 23, pp. 7318-7322, 2007.
[14] H. Khan and D. Berk, "Sol–gel synthesized vanadium doped TiO_2 photocatalyst: physicochemical properties and visible light photocatalytic studies", *Journal of Sol-Gel Science and Technology*, vol. 68, no. 2, pp. 180-192, 2013.
[15] C. C. Mercado, F.J. Knorr and J. L. McHale, "Observation of charge transport in single titanium dioxide nanotubes by micro-photoluminescence imaging and spectroscopy", *ACS Nano*, vol. 6, no. 8, pp. 7270-7280, 2012.
[16] H. E. Chao, Y. U. Yun, H. U. Xingfang and A. Larbot, "Effect of silver doping on the phase transformation and grain growth of sol-gel titania powder", *Journal of the European Ceramic Society*, vol. 23, no. 9, pp. 1457-1464, 2003.